Methylammonium Lead Bromide Perovskite Light Emitting Diodes by Chemical Vapor Deposition

*Matthew R. Leyden,[1]† Lingqiang Meng,[1]†, Yan Jiang,[1], Luis K. Ono[1], Longbin Qiu,[1] Emilio J. Juarez-Perez,[1]Chuanjiang Qin,[2] Chihaya Adachi,[2] and Yabing Qi [1]**

[1] Energy Materials and Surface Sciences Unit (EMSS), Okinawa Institute of Science and Technology Graduate University (OIST), 1919-1 Tancha, Onna-son, Kunigami-gun, Okinawa 904-0495, Japan

[2] Center for Organic Photonics and Electronics Research (OPERA),

Kyushu University, 744 Motooka, Nishi-ku, Fukuoka 819-0395, Japan

AUTHOR INFORMATION

†These authors contributed equally to this work.

*Corresponding Author: Yabing Qi, email: Yabing.Qi@OIST.jp

ABSTRACT

Organo-lead-halide perovskites are promising materials for optoelectronic applications. Perovskite solar cells have reached power conversion efficiencies over 22% and perovskite light emitting diodes have recently achieved over 11% external quantum efficiency. To date, most research on perovskite light emitting diodes has focused on solution processed films. There are many advantages of a vapor based growth process to prepare perovskite, including ease of patterning, ability to batch process, and material compatibility. We investigated an all vapor perovskite growth process by chemical vapor deposition and demonstrated luminance up to 560 cd/m^2.

TOC GRAPHICS

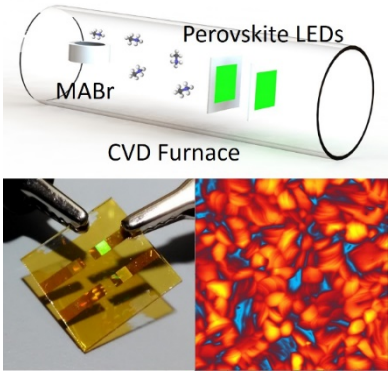

Perhaps best known for its solar cell applications, organo-lead-halide perovskite materials have demonstrated power conversion efficiencies reaching over 22%. In addition, perovskite materials are also promising as a light-emitting materials for light emitting diodes (LEDs) and lasers due to their high color purity, tunable bandgap, high and balanced carrier mobility both for electrons and holes.[1] Perovskites materials for LED applications have a slightly longer history than for solar cells. In 1994 researchers investigated low dimensional perovskite materials and were able to make bright LEDs with luminance over 10,000 cd/m^2, but only at liquid nitrogen temperatures.[2] In 1999 researchers demonstrated a low dimensional perovskite LED that functioned at room temperature with low efficiency.[3] In 2014, after the resurgence of interest in perovskite materials due to the rapid rise in solar cell performance, new reports appeared demonstrating electroluminescence at room temperature.[4,5] Since then there have been many reports demonstrating bright electroluminescence (~10,000 to 65,000 cd/m^2) using 3D perovskites,[6,7] and high external quantum efficiencies using low dimensional perovskites (EQE 8-11.7%).[8–12] Most of these reports used a methylammonium (MA) cation. Recently a report using formamidinium showed reasonably high efficiency.[13] Formamidinium may be a relevant choice as it has shown improved thermal stability in solar cells.

In solar cells applications, perovskite thin films generally have grain sizes that are hundreds of nanometers to microns. Larger grains provide easier charge separation and extraction. However, in LED applications perovskite films are typically engineered with small grains that confine injected charges and promote radiative recombination, as well as reduce surface roughness. There are several reports on how bright LED can be made by limiting grain size, including the nanocrystal pinning method, which uses an anti-solvent containing organic molecules to limit grain growth.[6] This method used an excess of MABr in solution, but MA can also be incorporated into

the film by a vapor process also yielding bright LEDs.[7] An excess of MABr has been shown to form isolated perovskite nanocrystals in a matrix of MABr,[14] where the resulting $MAPbBr_3$ films have a green color. Another method of controlling the grain size is to introduce a long ligand into the precursor solution.[8–12] This ligand is too big to fit into perovskite bulk structure and will define the grain boundary. By controlling the ratio of ligand to bulk material the crystal size can be tailored to the optimum geometry. Films made in this way typically contain the 3D perovskite structure, but as they are limited in size they might be called "low dimensional perovskites".

Most works on perovskite used solution processing techniques to form the perovskite layer for LED applications. A vapor process may be desirable in perovskite LED applications for many reasons, such as ease of patterning, improved uniformity, and material compatibility. There are currently a number of published works on chemical vapor deposition (CVD) of perovskite for solar cell applications.[15–18] However, to our knowledge, there is only one work that used a vapor deposition process for the LED application using $MAPbI_3$.[19] Additionally, there is a relevant set of example works that grow perovskite nano-crystals by chemical vapor deposition to demonstrate optically pumped lasing with at pump fluence down to 11 $\mu J/cm^2$ for $MAPbI_3$ and 20 $\mu J/cm^2$ for $MAPbBr_3$.[20,21]

In this work the perovskite layer was deposited with a two-step vapor process, i.e., the vacuum thermal evaporation of $PbBr_2$, which was followed by the chemical vapor deposition step to convert $PbBr_2$ to $MAPbBr_3$. The optimized film was smooth with surface roughness under 10 nm. To fabricate LEDs we used a work function modifying polymer PFN-OX (6,6'-(9',9'-Bis(6-((3-ethyloxetan-3-yl)methoxy)hexyl)-7,7'-diphenyl-9H,9'H-2,2'-bifluorene-9,9-diyl) bis(N,Ndiethylhexan-1-amine)) on indium tin oxide (ITO) as an electron injection layer. Using this structure, CVD LEDs reached a maximum luminance of 560 cd/m^2, with an EQE of ~0.016%.

This was a modest first step for chemical vapor deposited perovskite LEDs, but proves that it is possible to vapor deposit perovskite for LED applications and potentially opens the door for future research with potential advantages to scaling up production of large area LEDs and modules.

Prior to the CVD growth process substrates were first coated with a thin film of lead bromide by vacuum deposition. These substrates were then loaded into a 2-zone low pressure CVD furnace. MABr vapor was sublimated in one zone and deposited onto the next zone held at a lower temperature. After the conversion process, we observed that the films increased in thickness by a factor of ~2.2. The densities of $MAPbBr_3$ and $PbBr_2$ are 3.83 gram/cm^3 and 6.66 g/cm^3,[22] and have molecular weights of 479 g/mol and 367 g/mol, respectively. We expected to see a volume expansion of 2.27, which agreed with our observations and suggested that films are fully converted after the CVD process. Our first attempts to make $MAPbBr_3$ films were for solar cell applications. These films were 300 nm thick and grown with a substrate temperature of 120 °C. From initial growth optimization we fabricated solar cells reaching an efficiency of 5.3% (Fig. S1). Substrate temperatures significantly higher than 120 °C were not observed to convert $PbBr_2$ to perovskite (Fig. S2).

Using the growth recipe of $MAPbBr_3$ optimized for solar cells we could fabricate LEDs with luminance over 100 cd/m^2. However, these LEDs were typically short lived and relatively dim. To improve performance, we reduced grain size and film thickness without introducing pinholes into the film. We found that the most important parameter to controlling the surface roughness and grain size was the substrate growth temperature during the conversion process of MAPbBr3 when MABr is deposited onto $PbBr_2$ films. In ideal grain growth the size of the grain d, will follow $d \propto (Kt+d_o^2)^{1/2}$, where $K \propto \exp(-E/RT)$, t is time, E is activation energy, R is the Gas constant, and T is the temperature.[23] In this experiment we kept the time constant, and varied the temperature.

Reducing the temperature reduces the growth constant K, resulting in smaller grains. Additionally, we reduced the film thickness to constrain the grain growth in the direction perpendicular to the substrate. In this growth mode, the surface energy was more relevant as it prevented the crystallites from growing isotropically. By using atomic force microscopy (AFM) we showed that by reducing the thickness and growth temperature we are able to reduce the apparent grain size starting from our solar cell growth recipe that was a 300 nm thick film grown at 120 °C with an apparent grain size of ~300 nm, down to 125 nm for 100 nm films grown at 70 °C (Fig. 1). Grain boundaries were defined using a watershed technique using the software Gwyddion (Fig. S3). Reducing the film thickness further is possible, however we found that below a thickness of ~70 nm the surface energy was not sufficient to maintain the larger anisotropy and films were prone to forming pinholes when grown at temperatures of 90 °C (Fig 1g). To ensure that our films were pinhole free, films used for LED applications were grown at a thickness of 100 nm.

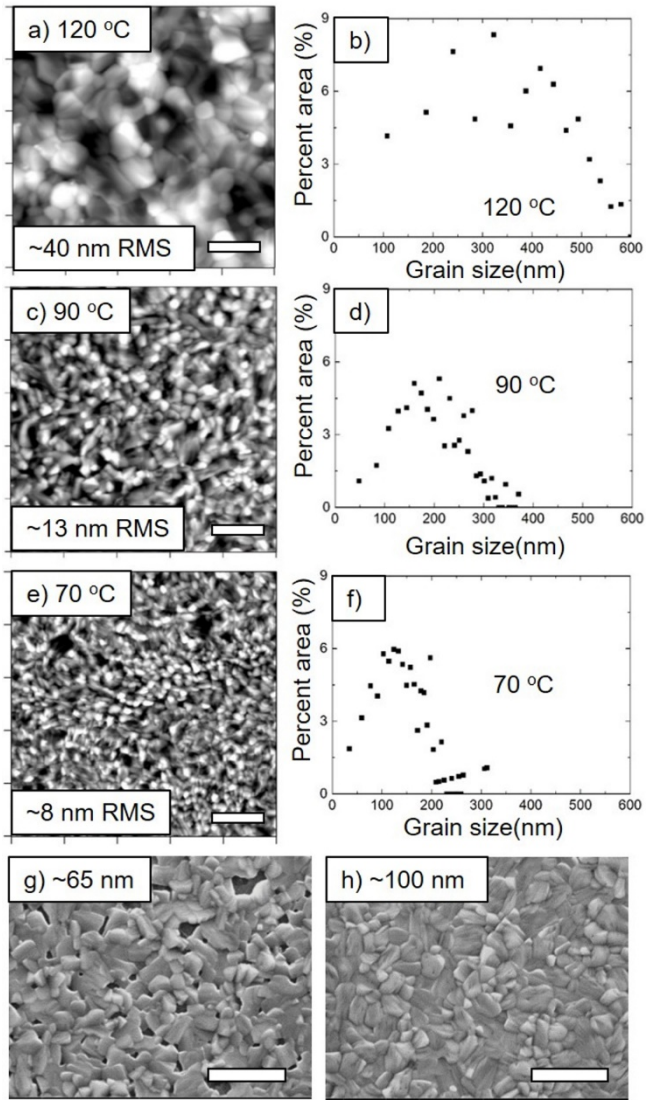

Figure 1. Substrate growth temperature and thickness determine grain size. The morphology of CVD grown $MAPbBr_3$ films were measured by AFM (a,c,e), with corresponding grain size distribution plotted in (b,d,f). a) 300 nm perovskite grown at 120 °C. c) 100 nm perovskite grown at 90 °C, e) 100 nm perovskite grown at 70 °C. g) SEM image of ~65 nm perovskite showing pinholes. H) SEM image of 100 nm perovskite grown at 90 °C showing complete coverage of the surface. The scale bar for all images is 1 μm.

We measured X-ray diffraction (XRD) spectra of our films and confirmed a reduction in crystallite size. Here we differentiate apparent grain size measured by AFM from crystallite size, as XRD measures crystalline material. Figure 2a shows the apparent grain size from 2 films as measured by AFM, and Fig. 2b the XRD spectra from analogous films. The reduction in grain size was evident by an increased full width half maximum (FWHM) of the peaks. The grain size can be estimated from the Scherrer equation where the crystal size is proportional to the inverse of the peak broadening minus the instrument broadening. We made a crude estimate of the broadening from the instrument by measuring a highly crystalline KCl powder (Fig. S4). It should be noted that this approach may not work well for crystallites over 100 nm, and is only used to give rough qualitative agreement between AFM data and XRD data. From the FWHM of the $MAPbBr_3$ (100) peak we can estimate an isometric crystal size ratio of 2.6, using the average 2θ FWHM obtained from KCl of 0.12^o. This corresponds to a volume ratio of ~18:1, however the volume ratio based on the apparent grain size from AFM was ~8:1. This discrepancy suggests that the films grown at low temperature with a wide aspect ratio could be polycrystalline. We also saw a reduction in the integrated area of this peak by a factor of 4.7. The integrated intensity should be proportional to the total crystalline volume of the film and is reasonably consistent with a 3-fold reduction in thickness.

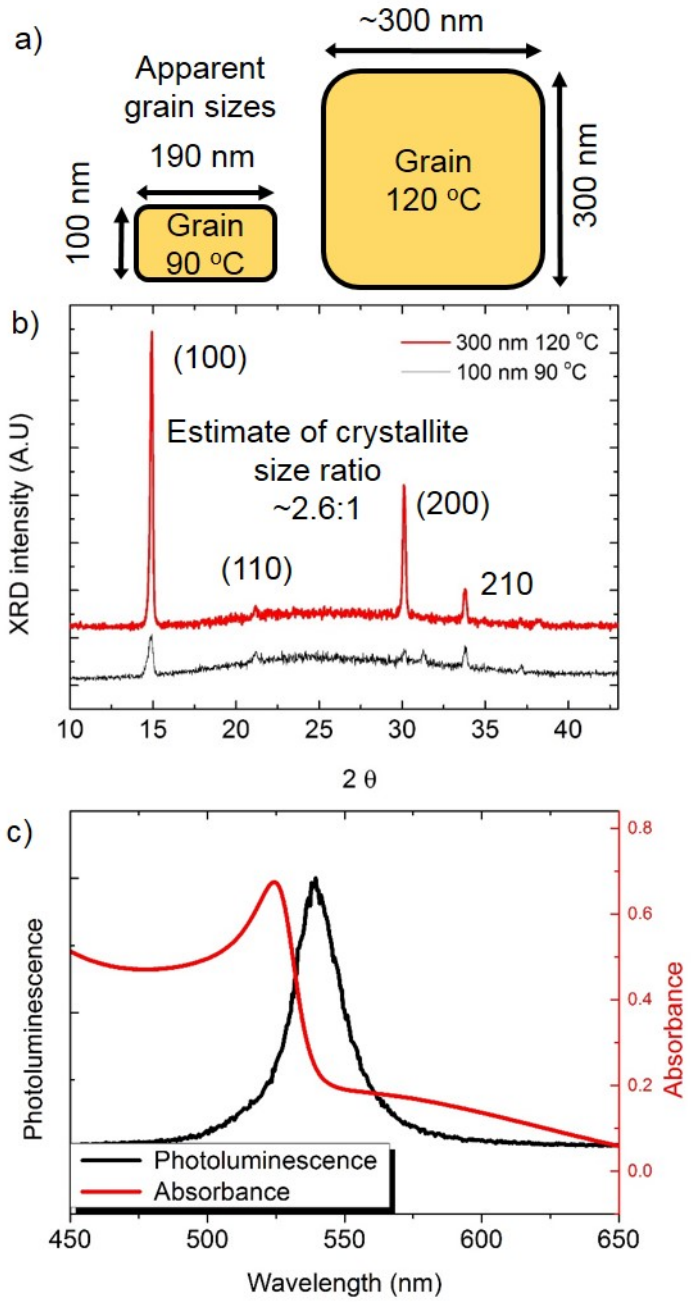

Figure 2. Characterization of CVD grown $MAPbBr_3$ films. Both AFM data and XRD data showed smaller grain sizes at lower growth temperatures a) The diagram shows the apparent grain size as measured by AFM of a 100 nm thin film grown at 90 °C and a 300 nm film grown at 120 °C. B) XRD spectra of films grown at 90 °C and 120 °C. The ratio of full width maxima of these two peaks was 2.6:1 with an assumed instrument broadening of 2θ equal to 0.12°. c) Absorption and

photoluminescence of 100 nm thick $MAPbBr_3$ CVD perovskite films. The absorption edge showed a distinctive excitonic peak that is typical of $MAPbBr_3$ films. The photoluminescent peak and absorption edge were both ~540 nm.

From absorption spectroscopy we saw an absorption edge at 540 nm, which was consistent with the measured photoluminescent peak (Fig. 2c). Exciton binding energy in $MAPbI_3$ perovskite is similar to or below thermal energy, while the exciton binding energy for $MAPbBr_3$ is higher and more relevant at room temperature ($MAPbBr_3$ ~40-150 meV)[24,25] An excitonic peak is clearly visible in the absorption spectrum seen in Fig 2c. Lead trihalide perovskite materials have relatively low exciton binding energy compared to other organic semiconductors, and may be more prone to dissociating rather than radiatively recombining.

Using ultra-violet photoelectron spectroscopy (UPS) we measured $MAPbBr_3$ perovskite to have a work function of 4.6 eV and an ionization energy value of 5.6 eV (Fig. 3). Using the absorption edge of 2.3 eV (Fig. 2) the conduction band minimum was located at ~3.3 eV below the vacuum level. Considering the conduction band level of the $MAPbBr_3$, we tried PFN-OX as a surface modification layer for ITO electrodes, which was reported in organic LEDs to have a work function of 3.4 eV.[26] We measured our ITO/PFN-OX films to have a work function of 3.5 eV, which was consistent with expectations, and completed LEDs performed well compared to other electron transport films tried. Based on UPS and absorption spectra PFN-OX acts as a work function modifier and not a hole blocking layer (Fig. S5). We used 20 nm of TAPC (4,4′ -Cyclohexylidenebis[*N*,*N*-bis(4-methylphenyl]benzenamine) as the hole transport layer, 10 nm of MoO_3 as the hole injection layer, and gold as the anode. This structure is commonly used for hole injection in organic LEDs. Detailed UPS data for all layers can be found in Fig. S6.

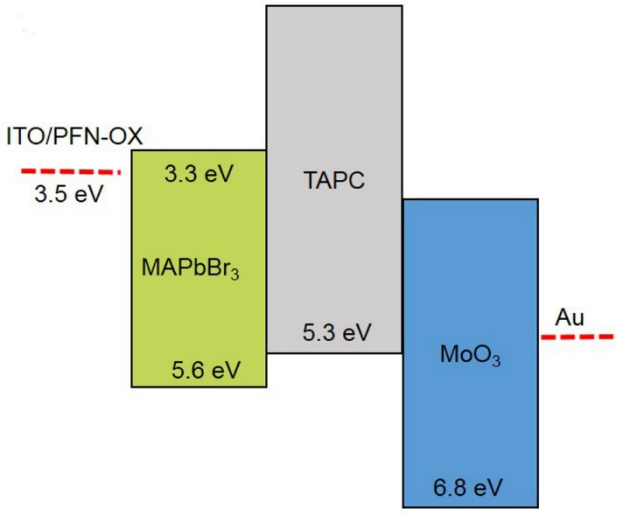

Figure 3. Band energy alignment in CVD grown perovskite LEDs. The LED structure ITO/PFN-OX/$MAPbBr_3$/TAPC/MoO_3/Au, with relevant work functions (red dashes), conduction and valence bands of the perovskite, TAPC, and MoO_3.

The optimized film growth condition was found at 100 nm of perovskite grown at 90 °C. This film reached a maximum luminance of 340 cd/m^2, with an EQE of 0.01% (Fig. 4). Despite having smoother films with smaller apparent grain sizes, we did not see higher performance when the films were grown at 70 °C. The best performing LED grown at 70 °C had a maximum luminescence of ~120 cd/m^2 (Fig. S7). We first thought that this lower performance was because on average growths at 70 °C were more prone to incomplete perovskite formation. However, as measured by XRD films grown at 70 °C had comparable crystallinity to those grown at 90 °C, and differences may have been smaller than the error in our measurement. Even optimized LEDs appeared limited by trap states at low bias voltages and have very low EQE. When operating LEDs at higher current densities trap states filled causing the EQE and luminance to rise. However, these high current densities were not sustainable and LEDs non-reversibly dropped in performance due to overheating when current densities were higher than ~800 mA/cm^2. In this work the perovskite film growth was largely controlled by temperature, and because of this there was a compromise

between crystallite size and crystallite quality. A long growth at high temperature will result in larger high quality crystallites. However large grains allow for exciton dissociation. By reducing the temperature we could reduce the grain size promoting radiative recombination, but this condition likely led to the reduction of crystallite quality potentially increased trap state density. An additional mechanism is needed to either improve crystallite quality without increasing grain size or limit grain size with a low dependence on growth temperature. One promising approach to limit grain size would include a large ligand into the perovskite CVD process forming low dimensional perovskite crystallites. In this way crystallite size is controlled by molecular stoichiometry, and not only by processing conditions.

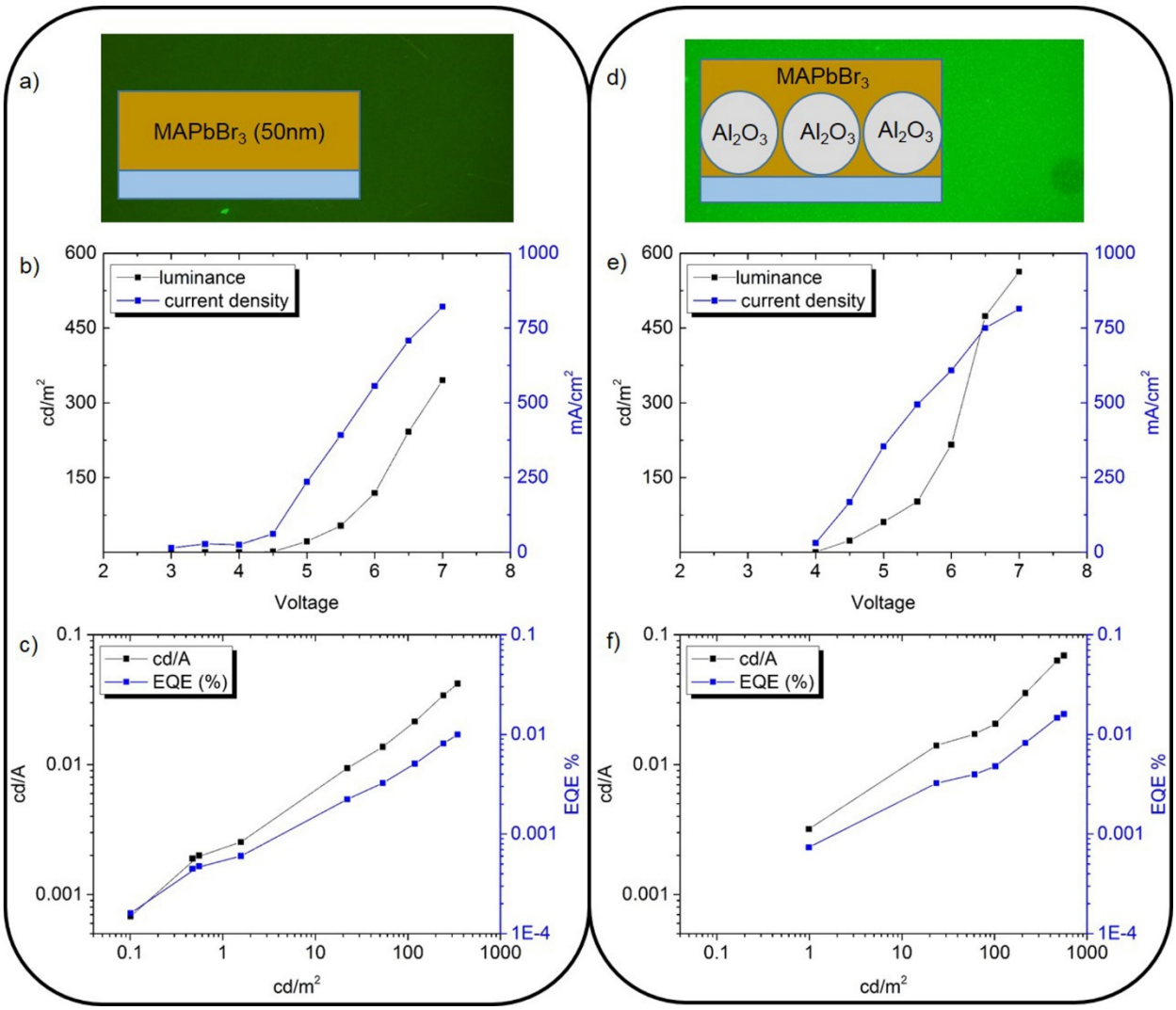

Figure 4. Alumina nanoparticles in the perovskite film improved fluorescence and electroluminescence. Fluorescent microscope images of a) 50 nm film of $MAPbBr_3$ and d) an equivalent volume of $MAPbr_3$ grown in a matrix of 50 nm alumina nanoparticles. The images were taken at the same magnification and exposure time to show that the alumina nanoparticles increased the fluorescent intensity of the film. b-c) Performance of a CVD grown 100 nm $MAPbBr_3$ LED. e-f) Shows the improved performance in an analogous film grown using a 50 nm alumina matrix.

We found that we could improve performance of the LEDs by incorporating a monolayer of alumina nanoparticles (size < 50 nm, Sigma Aldrich) into the thin film of perovskite. Initially we observed that thin films of $MAPbBr_3$ grown on alumina scaffold had brighter photoluminescence as observed by fluorescent microscopy (Fig 4 a,d). After incorporating the alumina scaffold into the LED structure we also saw an improvement in LED performance (Fig 4 e and f). To elucidate the role of alumina in film growth we measured photoluminescence of perovskite films on quartz, ITO, and ITO with alumina. The film grown on the ITO-alumina substrate had higher intensity than either the films grown on quartz or ITO alone. The alumina nanoparticles are chemically inert, but likely acted as a morphology regulator that limited grain size and increased photoluminescent intensity. Additionally, the alumina also minimized quenching effects by electrically isolating the perovskite grains from direct contact with ITO. The film grown directly on ITO showed lower intensity than the film grown on quartz. (Fig S8). This approach is somewhat analogous to a report that used a polymer matrix to hold the perovskite emitter material.[27] Despite having higher photoluminescent intensity and higher luminance LEDs we did not observe a significant difference in the photoluminescent lifetimes between PFN-OX/alumina films and PFN-OX only films (Fig. S8).

At lower applied voltages the LED typically had a broad color emission rather than a pure green. This broad band emission can be seen more clearly in Fig. 5a. We saw at ~5 V the formation of a broad band emission that peaked at the short wavelength edge ~425 nm. The most likely source of this was the hole transport layer TAPC. By itself, TAPC has a broad luminescence peak around 450 nm and a more defined peak at 600 nm, however this can be shifted depending on the neighbouring thin films.[28] At higher bias voltages this broad peak decreased while the peak from the perovskite increased, and the broad peak was essentially gone by 7 V. We replaced TAPC

with a different hole transport layer TPT1 (1,1-biphenyl-4-yl-*N*,*N*-dipheny-1-1,1-biphenyl, TPT1),[29] and did not see any emission other than the perovskite, confirming that the broad emission was likely from the TAPC (Fig. S9).

One important advantage of organo-lead-halide perovskite materials is the ability to tune their band gap. It is possible to tune the emission of perovskites throughout most of the visible spectrum (390 to 790 nm).[1] In this work we did not test the entire visible spectrum, but simply demonstrated the tuning of the emission wavelength is possible using a CVD based perovskite growth process. We sublimated MACl in the CVD process in place of MABr onto substrates coated with a $PbBr_2$ thin film for a resultant film of $MAPbBr_{(3-x)}Cl_x$. The inclusion of chlorine into the perovskite lattice was evident by the blue shifted emission of the perovskite LED from ~530 to ~510 nm (Fig. 5b). Chlorine appeared to have low affinity to replace bromine in the perovskite lattice, and we expected x= ~1 for formation of $MAPbBr_2Cl$. The electroluminescence was consistent with the photoluminescence peak of 514 nm reported in another work.[30]

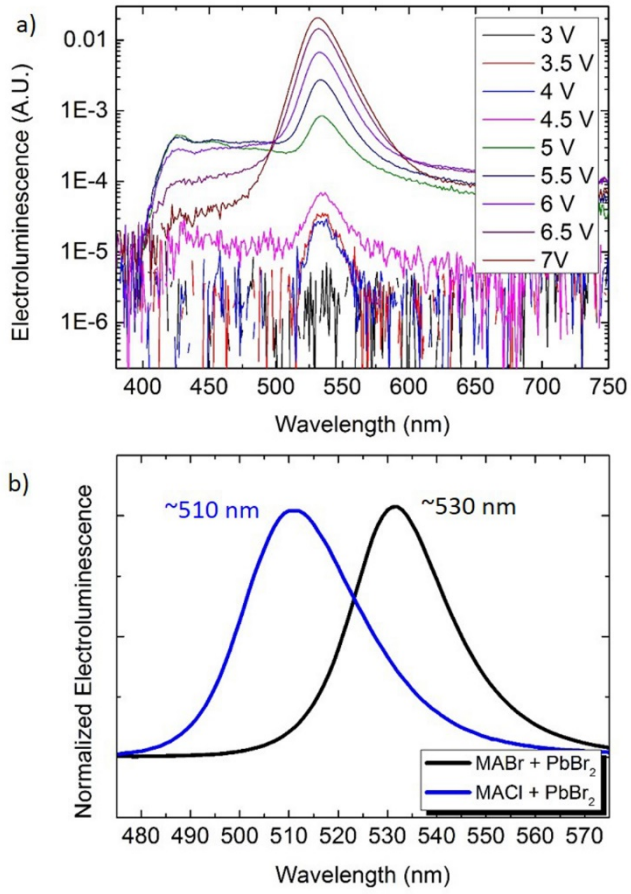

Figure 5. Electroluminescence spectra of CVD grown perovskite LEDs. a) Emission spectra of the structure shown in Figures 3, 4b and 4c as a function of applied voltage. We saw at ~3.5 V there was a low intensity emission from the perovskite layer. At 5 V there was an emission from the perovskite layer as well as a broad emission that likely originated from TAPC, peaking at ~425 nm. At 7 V the broad band emission disappeared. b) Normalized electroluminescent spectra from a completed $MAPbBr_3$ LED (emission ~532 nm) and a CVD growth using MACl precursor, forming ~$MAPbBr_2Cl$ (emission ~511 nm). This growth clearly showed blue shifted electroluminescence due to the contraction of the lattice from inclusion of chlorine.

Chemical vapor deposition of perovskites is a promising alternative to solution based methods of fabrication due to the relative ease of patterning, ability to batch process, wide range of material

compatibility, and potential for uniform large area deposition. Previous work using CVD demonstrated large area perovskite growth, where films are prepared in multi-substrate batches.[17] This work also showed that by pre-patterning, the perovskite shunt resistance in resultant modules was improved. A vapor process offers material compatibility with sensitive device structures that may otherwise react or dissolve in a solution based process. For example, the electron injection layer PFN-OX used in this work was found to be incompatible with perovskite formed by solution processing. An example of a larger area LED grown by CVD is shown in Fig. S10. In this work we fabricated $MAPbBr_3$ films with surface roughness under 10 nm and demonstrated LEDs with luminance up to 560 cd/m^2. There are very few works focusing on vapor deposited perovskite light emitting diodes, and based on recent progress within the perovskite field there is likely significant room for improvement.

ACKNOWLEDGMENT

This work was supported by funding from the Energy Materials and Surface Sciences Unit of the Okinawa Institute of Science and Technology Graduate University, the OIST Proof of Concept (POC) Program, the OIST R&D Cluster Research Program, and JSPS KAKENHI Grant Number 15K17925.

SUPPORTING INFORMATION

Experimental procedures and additional characterization.

REFERENCES

(1) Sutherland, B. R.; Sargent, E. H. Perovskite Photonic Sources. *Nat. Photonics* **2016**, *10*, 295–302.
(2) Era, M.; Morimoto, T.; Saito, S. Organic-inorganic Heterostructure Electroluminescent Device Using a Layered Perovskite Semiconductor (C6H5C2H4NH3)2PbI4. *Appl. Phys. Lett.* **1994**, *65*, 676–678.

(3) Chondroudis, K.; Mitzi, D. B. Electroluminescence from an Organic–Inorganic Perovskite Incorporating a Quaterthiophene Dye within Lead Halide Perovskite Layers. *Chem. Mater.* **1999**, *11*, 3028–3030.
(4) Tan, Z.-K.; Moghaddam, R. S.; Lai, M. L.; Docampo, P.; Higler, R.; Deschler, F.; Price, M.; Sadhanala, A.; Pazos, L. M.; Credgington, D.; et al. Bright Light-Emitting Diodes Based on Organometal Halide Perovskite. *Nat. Nanotechnol.* **2014**, *9*, 687–692.
(5) Kim, Y.-H.; Cho, H.; Lee, T.-W. Metal Halide Perovskite Light Emitters. *Proc. Natl. Acad. Sci.* **2016**, *113*, 11694–11702.
(6) Cho, H.; Jeong, S.-H.; Park, M.-H.; Kim, Y.-H.; Wolf, C.; Lee, C.-L.; Heo, J. H.; Sadhanala, A.; Myoung, N.; Yoo, S.; et al. Overcoming the Electroluminescence Efficiency Limitations of Perovskite Light-Emitting Diodes. *Science* **2015**, *350*, 1222.
(7) Chih, Y.-K.; Wang, J.-C.; Yang, R.-T.; Liu, C.-C.; Chang, Y.-C.; Fu, Y.-S.; Lai, W.-C.; Chen, P.; Wen, T.-C.; Huang, Y.-C.; et al. NiOx Electrode Interlayer and CH3NH2/CH3NH3PbBr3 Interface Treatment to Markedly Advance Hybrid Perovskite-Based Light-Emitting Diodes. *Adv. Mater.* **2016**, *28*, 8687–8694.
(8) Yuan, M.; Quan, L. N.; Comin, R.; Walters, G.; Sabatini, R.; Voznyy, O.; Hoogland, S.; Zhao, Y.; Beauregard, E. M.; Kanjanaboos, P.; et al. Perovskite Energy Funnels for Efficient Light-Emitting Diodes. *Nat. Nanotechnol.* **2016**, *11*, 872–877.
(9) Wang, N.; Cheng, L.; Ge, R.; Zhang, S.; Miao, Y.; Zou, W.; Yi, C.; Sun, Y.; Cao, Y.; Yang, R.; et al. Perovskite Light-Emitting Diodes Based on Solution-Processed Self-Organized Multiple Quantum Wells. *Nat. Photonics* **2016**, *10*, 699–704.
(10) Byun, J.; Cho, H.; Wolf, C.; Jang, M.; Sadhanala, A.; Friend, R. H.; Yang, H.; Lee, T.-W. Efficient Visible Quasi-2D Perovskite Light-Emitting Diodes. *Adv. Mater.* **2016**, *28*, 7515–7520.
(11) Xiao, Z.; Kerner, R. A.; Zhao, L.; Tran, N. L.; Lee, K. M.; Koh, T.-W.; Scholes, G. D.; Rand, B. P. Efficient Perovskite Light-Emitting Diodes Featuring Nanometre-Sized Crystallites. *Nat. Photonics* **2017**, *11*, 108–115.
(12) Seo, H.-K.; Kim, H.; Lee, J.; Park, M.-H.; Jeong, S.-H.; Kim, Y.-H.; Kwon, S.-J.; Han, T.-H.; Yoo, S.; Lee, T.-W. Efficient Flexible Organic/Inorganic Hybrid Perovskite Light-Emitting Diodes Based on Graphene Anode. *Adv. Mater.* **2017**, *29*, 1605587.1-1605587.6.
(13) Meng, L.; Yao, E.-P.; Hong, Z.; Chen, H.; Sun, P.; Yang, Z.; Li, G.; Yang, Y. Pure Formamidinium-Based Perovskite Light-Emitting Diodes with High Efficiency and Low Driving Voltage. *Adv. Mater.* **2017**, *29*, 1603826.1-1603826.7.
(14) Lee, J.-W.; Choi, Y. J.; Yang, J.-M.; Ham, S.; Jeon, S. K.; Lee, J. Y.; Song, Y.-H.; Ji, E. K.; Yoon, D.-H.; Seo, S.; et al. In-Situ Formed Type I Nanocrystalline Perovskite Film for Highly Efficient Light-Emitting Diode. *ACS Nano* **2017**, *11*, 3311–3319.
(15) Leyden, M. R.; Ono, L. K.; Raga, S. R.; Kato, Y.; Wang, S.; Qi, Y. B. High Performance Perovskite Solar Cells by Hybrid Chemical Vapor Deposition. *J. Mater. Chem. A* **2014**, *2*, 18742–18745.
(16) Leyden, M. R.; Lee, M. V.; Raga, S. R.; Qi, Y. B. Large Formamidinium Lead Trihalide Perovskite Solar Cells Using Chemical Vapor Deposition with High Reproducibility and Tunable Chlorine Concentrations. *J. Mater. Chem. A* **2015**, *3*, 16097–16103.
(17) Leyden, M. R.; Jiang, Y.; Qi, Y. B. Chemical Vapor Deposition Grown Formamidinium Perovskite Solar Modules with High Steady State Power and Thermal Stability. *J. Mater. Chem. A* **2016**, *4*, 13125–13132.

(18) Ono, L. K.; Leyden, M. R.; Wang, S.; Qi, Y. B. Organometal Halide Perovskite Thin Films and Solar Cells by Vapor Deposition. *J. Mater. Chem. A* **2016**, *4*, 6693–6713.
(19) Gil-Escrig, L.; Miquel-Sempere, A.; Sessolo, M.; Bolink, H. J. Mixed Iodide–Bromide Methylammonium Lead Perovskite-Based Diodes for Light Emission and Photovoltaics. *J. Phys. Chem. Lett.* **2015**, *6*, 3743–3748.
(20) Zhang, Q.; Ha, S. T.; Liu, X.; Sum, T. C.; Xiong, Q. Room-Temperature Near-Infrared High-Q Perovskite Whispering-Gallery Planar Nanolasers. *Nano Lett.* **2014**, *14*, 5995–6001.
(21) Xing, J.; Liu, X. F.; Zhang, Q.; Ha, S. T.; Yuan, Y. W.; Shen, C.; Sum, T. C.; Xiong, Q. Vapor Phase Synthesis of Organometal Halide Perovskite Nanowires for Tunable Room-Temperature Nanolasers. *Nano Lett.* **2015**, *15*, 4571–4577.
(22) Weber, D. CH3NH3PbX3, a Pb(II)-System with Cubic Perovskite Structure. *Z Naturforsch* **1978**, *33 b*, 1443–1445.
(23) Rollett, A.; Humphreys, F. J.; Rohrer, G. S.; Hatherly, M. *Recrystallization and Related Annealing Phenomena*; Elsevier, Oxford, UK, 2004.
(24) Koutselas, I. B.; Ducasse, L.; Papavassiliou, G. C. Electronic Properties of Three- and Low-Dimensional Semiconducting Materials with Pb Halide and Sn Halide Units. *J. Phys. Condens. Matter* **1996**, *8*, 1217.
(25) Yang, Y.; Yang, M.; Li, Z.; Crisp, R.; Zhu, K.; Beard, M. C. Comparison of Recombination Dynamics in CH3NH3PbBr3 and CH3NH3PbI3 Perovskite Films: Influence of Exciton Binding Energy. *J. Phys. Chem. Lett.* **2015**, *6*, 4688–4692.
(26) Zhang, K.; Zhong, C.; Liu, S.; Liang, A.; Dong, S.; Huang, F. High Efficiency Solution Processed Inverted White Organic Light Emitting Diodes with a Cross-Linkable Amino-Functionalized Polyfluorene as a Cathode Interlayer. *J. Mater. Chem. C* **2014**, *2*, 3270–3277.
(27) Li, G.; Tan, Z.-K.; Di, D.; Lai, M. L.; Jiang, L.; Lim, J. H.-W.; Friend, R. H.; Greenham, N. C. Efficient Light-Emitting Diodes Based on Nanocrystalline Perovskite in a Dielectric Polymer Matrix. *Nano Lett.* **2015**, *15*, 2640–2644.
(28) Yang, S.; Jiang, M. White Light Generation Combining Emissions from Exciplex, Excimer and Electromer in TAPC-Based Organic Light-Emitting Diodes. *Chem. Phys. Lett.* **2009**, *484*, 54–58.
(29) Aonuma, M.; Oyamada, T.; Sasabe, H.; Miki, T.; Adachi, C. Material Design of Hole Transport Materials Capable of Thick-Film Formation in Organic Light Emitting Diodes. *Appl. Phys. Lett.* **2007**, *90*, 183503.1-183503.3.
(30) Vega, E.; Mollar, M.; Marí, B. Synthesis of MAPbBr3-IYi (Y=I, Cl and I=0, 1, 2, 3) Thin Film Perovskites. *Phys. Status Solidi C* **2016**, *13*, 30–34.